



Killing Two Birds with One Stone: Discovery of Dual Inhibitors of Oxygen and Fumarate Respiration in Zoonotic Parasite, *Echinococcus multilocularis*

Shigehiro Enkai,^{a,b} Hirokazu Kouguchi,^c Daniel Ken Inaoka,^{b,d,e} Tomoo Shiba,^f Masahito Hidaka,^c Hiroyuki Matsuyama,^c Takaya Sakura,^{b,d} Kinpei Yagi,^{c,g} Kiyoshi Kita^{b,e,h}

^aDepartment of Pediatrics, Teikyo University School of Medicine, Tokyo, Japan

^bSchool of Tropical Medicine and Global Health, Nagasaki University, Nagasaki, Japan

^cDepartment of Infectious Diseases, Hokkaido Institute of Public Health, Sapporo, Hokkaido, Japan

^dDepartment of Molecular Infection Dynamics, Shionogi Global Infectious Diseases Division, Institute of Tropical Medicine (NEKKEN), Nagasaki University, Nagasaki, Japan

^eDepartment of Biomedical Chemistry, Graduate School of Medicine, The University of Tokyo, Tokyo, Japan

^fDepartment of Applied Biology, Graduate School of Science Technology, Kyoto Institute of Technology, Kyoto, Japan

^gLaboratory of Parasitology, Department of Disease Control Faculty of Veterinary Medicine, Hokkaido University, Sapporo, Hokkaido, Japan

^hDepartment of Host-Defense Biochemistry, Institute of Tropical Medicine (NEKKEN), Nagasaki University, Nagasaki, Japan

ABSTRACT Ascofuranone (AF), a meroterpenoid isolated from various filamentous fungi, including *Acremonium egyptiacum*, has been reported as a potential lead candidate for drug development against parasites and cancer. In this study, we demonstrated that AF and its derivatives are potent anthelmintic agents, particularly against *Echinococcus multilocularis*, which is the causative agent of alveolar echinococcosis. We measured the inhibitory activities of AF and its derivatives on the mitochondrial aerobic and anaerobic respiratory systems of *E. multilocularis* larvae. Several derivatives inhibited complex II (succinate:quinone reductase [SQR]; IC₅₀ = 0.037 to 0.135 μM) and also complex I to III (NADH:cytochrome *c* reductase; IC₅₀ = 0.008 to 0.401 μM), but not complex I (NADH:quinone reductase), indicating that mitochondrial complexes II and III are the targets. In particular, complex II inhibition in the anaerobic pathway was notable because *E. multilocularis* employs NADH:fumarate reductase (fumarate respiration), in addition to NADH oxidase (oxygen respiration), resulting in complete shutdown of ATP synthesis by oxidative phosphorylation. A structure-activity relationship study of *E. multilocularis* complex II revealed that the functional groups of AF are essential for inhibition. Binding mode prediction of AF derivatives to complex II indicated potential hydrophobic and hydrogen bond interactions between AF derivatives and amino acid residues within the quinone binding site. *Ex vivo* culture assays revealed that AF derivatives progressively reduced the viability of protoscolexes under both aerobic and anaerobic conditions. These findings confirm that AF and its derivatives are the first dual inhibitors of fumarate and oxygen respiration in *E. multilocularis* and are potential lead compounds in the development of anti-echinococcal drugs.

KEYWORDS *Echinococcus multilocularis*, ascofuranone, structure-activity relationship, mitochondrial complex II, fumarate respiration, drug development, dual inhibitors

Alveolar echinococcosis is a chronic, progressive, and life-threatening parasitic disease that is caused by the larval metacystode stage of *Echinococcus multilocularis*. This parasite is a public health concern throughout the Northern Hemisphere. Currently, albendazole is the only available chemotherapy for alveolar echinococcosis and shows insufficient efficacy (1, 2). Therefore, echinococcosis has been designated as a neglected tropical disease, and the development of novel drugs is urgently required

Copyright © 2023 Enkai et al. This is an open-access article distributed under the terms of the [Creative Commons Attribution 4.0 International license](https://creativecommons.org/licenses/by/4.0/).

Address correspondence to Shigehiro Enkai, shigehiro.enkai@med.teikyo-u.ac.jp.

The authors declare no conflict of interest.

Received 24 October 2022

Returned for modification 2 December 2022

Accepted 3 January 2023

Published 22 February 2023

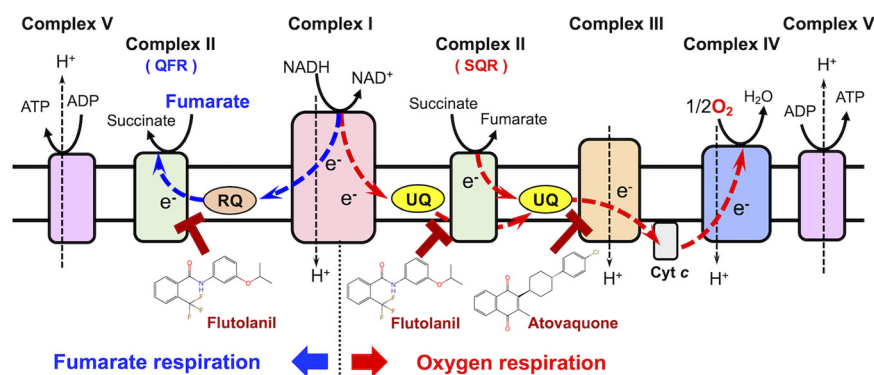


FIG 1 Overview of the mitochondrial respiratory chain of *E. multilocularis*. Fumarate respiration (NADH: fumarate reductase system) involves complex I, rhodoquinone (RQ), and complex II (quinol:fumarate reductase, QFR). In this system, electrons from NADH are transferred to RQ through complex I, and then transferred to fumarate by the QFR activity of complex II. An electrochemical gradient is maintained by the activity of complex I, and ATP is generated by oxidative phosphorylation (complex V) even under hypoxic conditions. Oxygen respiration is performed by complexes I, II, III, and IV, with ubiquinone (UQ) acting as an electron carrier between complexes I/II and III, and cytochrome *c* (Cyt *c*) between complexes III and IV. Complex II transfers electrons from succinate to UQ, acting as a succinate:quinone reductase (SQR). At the end of oxygen respiration, the electrons from NADH and succinate are used to reduce oxygen molecules to form water. Flutolanil and atovaquone are quinone binding site inhibitors of complexes II and III, respectively.

(3). As such, we focused on the mitochondrial respiratory chain of *E. multilocularis* as a drug target, and reported that atovaquone, a potent inhibitor of oxygen respiration that targets mitochondrial complex III (quinol:cytochrome *c* reductase), shows a synergic effect *ex vivo* and also *in vivo* when administered in combination with albendazole (4). Despite increasing evidence that the quinone binding sites of the mitochondrial respiratory complexes of the parasite are a potential target space, development has been challenging due to the plasticity of mitochondrial respiration. This plasticity allows the parasite to (i) alternate between oxygen and fumarate respiration, and (ii) rapidly adapt to the presence of individual respiratory inhibitors. In other words, one respiration mechanism being active is sufficient to maintain the electrochemical gradient that is required to synthesize ATP by oxidative phosphorylation, and facilitate parasite survival.

Oxygen respiration is driven by the activities of complexes I, II, III, and IV, which make up the mitochondrial electron transport chain (ETC). Complexes I (NADH:quinone oxidoreductase) and II (succinate:quinone reductase, SQR) transfer electrons from NADH and succinate, respectively, to complex III via the ubiquinone pool (Fig. 1). The reducing equivalents from the ubiquinone pool are transferred by complex III to complex IV via cytochrome *c*. At the end of the ETC, electrons are finally transferred to dioxygen, resulting in the production of water. In the aerobic pathway, complex III of *E. multilocularis* has been reported as a feasible and promising drug target for echinococcosis, because the antimalarial atovaquone strongly inhibits complex III in *E. multilocularis* and restricts the growth of larval cysts *in vivo* (5). Fumarate respiration involves mitochondrial complexes I and II, and plays an important role in the survival of *E. multilocularis* under hypoxic conditions in the host (6). Fumarate respiration is composed of complex I, low-potential electron mediator rhodoquinone (RQ), and the reverse reaction catalyzed by complex II (quinol:fumarate reductase [QFR]). The reducing equivalent from NADH is first transferred to RQ by complex I, and then from the reduced RQ to fumarate via the QFR activity of complex II, producing succinate (Fig. 1).

The electrochemical gradient that is formed during oxygen respiration is maintained by the proton pump activity of complexes I, III, and IV and is used by complex V to synthesize ATP. Although complex I becomes the sole respiratory complex to maintain the electrochemical gradient during fumarate respiration, it is capable of synthesizing ATP even in the absence of oxygen. Moreover, considering the internal hypoxic condition of

the hydatid cyst, fumarate respiration is likely predominant in *E. multilocularis* protoscolecetes, and both complex I and II have been suggested as drug targets (6, 7). In fact, quinazoline derivatives that inhibit *E. multilocularis* complex I effectively kill protoscolecetes in *ex vivo* assays (6). Given that quinazoline and its derivatives also inhibit mammalian complex I, the identification of selective inhibitors of parasite respiratory chain enzymes will be key in developing drugs for alveolar echinococcosis.

Ascofuranone (AF) is a meroterpenoid compound produced by filamentous fungi, including *Acremonium egyptiacum* (8, 9). AF has been reported to be an inhibitor of the quinone binding site of mitochondrial enzymes in various organisms, and it strongly inhibits the ubiquinol oxidase activity of *Trypanosoma brucei* mitochondrial alternative oxidase (TAO), an enzyme that is essential for parasite survival (10–13). Recent studies have shown that AF strongly inhibits the mitochondrial respiratory chain of *Schistosoma mansoni* and reduces the worm burden (14). Furthermore, AF and its derivatives do not inhibit mammalian respiratory chain complexes, although these compounds potently inhibit human dihydroorotate dehydrogenase (HsDHODH). This enzyme is the rate-limiting step of the pyrimidine *de novo* biosynthesis pathway, and inhibition of HsDHODH drastically reduces the viability of cancer cells, especially under tumor-microenvironment mimicking conditions (hypoxia and nutrient-deprivation) (15, 16). It has been reported that AF also suppresses the signaling pathways of invasion and migration in cancer cells (17, 18). Recently, the entire biosynthetic pathway of AF has been clarified in *A. egyptiacum* (19, 20); therefore, further manipulation of this strain could enable mass production of AF and its biosynthesis intermediates to perform *in vivo* experiments and evaluate its clinical applications.

Here, we report novel pharmacological findings of AF and its derivatives, which could contribute to the development of anti-echinococcal drugs as well as elucidate mitochondrial function in *E. multilocularis*. We examined the inhibitory activities of AF and its derivatives on the mitochondrial respiratory chain of *E. multilocularis* and evaluated their structure-activity relationship with complex II and their binding mode. In addition, we demonstrated the efficacy of AF derivatives against *E. multilocularis* protoscolecetes in *ex vivo* assays under aerobic and anaerobic conditions.

RESULTS

Effects of AF derivatives on the mitochondrial respiratory chain of *E. multilocularis*. Table 1 (see AF, D1 to 5) shows the inhibitory potency of AF and its derivatives against complexes I, II, and III. The NADH:ubiquinone reductase activity of complex I was not inhibited by AF or any of its derivatives. For the SQR activity of complex II, several derivatives showed inhibitory activity at low concentrations, $IC_{50} = 0.088$ to $0.135 \mu\text{M}$. The NADH:cytochrome *c* reductase activity by complexes I and III, was potently inhibited by AF derivatives, with IC_{50} values of 0.008 to $0.274 \mu\text{M}$. As complex I is not inhibited by AF or its derivatives, the target of inhibition is complex III. Notably, several AF derivatives inhibited both complexes II and III, although the inhibitory activity for each complex differed according to the structure of the compounds.

Structure-activity relationship of AF and its derivatives against complex II (SQR) of *E. multilocularis*. As the inhibition of complex II activity by AF and its derivatives can be examined directly, the structure-activity relationship of the compounds was examined. Structurally, AF is comprised of benzene, linker, and terminal groups (Fig. S1). Table 2 shows several AF derivatives with alterations in the benzene group that were evaluated (see AF, D5 to 11). Substitution of the aldehyde group (D7) increased the IC_{50} 2-fold compared to the acetyl group (D6), indicating that the 1-acetyl group is more favorable than the 1-aldehyde group for inhibiting SQR activity. When the acetyl group (D6) or 1-aldehyde group (D7) was changed to a methyl ester group (D9), the inhibitory activity was lost ($IC_{50} > 10 \mu\text{M}$), suggesting that substituents bulkier than an acetyl group are deleterious for the inhibition of SQR activity. Next, the contribution of the 5-Cl group was evaluated. A comparison between D7 and D8 revealed that the 5-Cl group is essential for the inhibitory activity. However, when the 6-methyl group was removed from the benzene ring, the inhibitory activity was

TABLE 1 Inhibitory effect of ascofuranone and representative derivatives on *E. multilocularis* protoscoleces mitochondria

ID	Compounds	IC ₅₀ (μM)		
		NADH:decyl rholoquinone reductase (complex I)	Succinate:quinone reductase (SQR) (complex II)	NADH:cytochrome c reductase (complex I and III)
AF		>50	1.10 ± 0.21	0.057 ± 0.011
D1		>50	0.088 ± 0.013	0.274 ± 0.025
D2		>50	0.309 ± 0.021	0.008 ± 0.002
D3		>50	0.135 ± 0.014	0.014 ± 0.002
D4		>50	0.037 ± 0.008	0.109 ± 0.009
D5		>50	0.047 ± 0.011	0.221 ± 0.044

increased by 2- to 3-fold (D5 and 6, AF and 10). In addition, when the 4-OH group in AF was changed to a methoxy group (as D11), the inhibitory activity was lost. The contribution of the 2-OH group for the inhibition of complex II could not be evaluated in this study because of difficulties in the synthesis of AF derivatives with substitutions only at this position.

The effect of the linker length of AF derivatives on SQR inhibition was also evaluated. As shown in Table 3, the optimum linker lengths for potent inhibition were observed at C7, C9, and C10 (IC₅₀ = 0.95, 1.2, and 1.2 μM, respectively). In contrast, compounds with either a short linker (C0, C3, and C5) or the longest one (C12) exhibited a remarkable decrease in potency. Modifications of the linker group were also evaluated (Table 4). Four types of linker chain were compared to clarify the function of the linker group. The IC₅₀ values of compounds D12 (geranyl chain), D13 (two branched methyl groups), D14 (one branched methyl group), and D15 (linear alkyl chain) were 0.57, 0.28, 0.54, and 0.89 μM, respectively. The IC₅₀ of D13 with two branched methyl groups was three times lower than that of D15, which had a linear alkyl chain.

AF derivatives possessing changes in the terminal group were also evaluated (Table 5). Changing the furanone ring to other groups, such as in D2, 16, and 17, resulted in IC₅₀ values decreasing to 0.30, 0.25, and 0.48 μM, respectively, compared with an IC₅₀ of 1.1 μM for AF. However, IC₅₀ was increased in several groups, such as D18 and 19.

Structural insights into the inhibition mechanism of complex II by AF derivatives. A structure prediction of *E. multilocularis* complex II was performed using AlphaFold2 (Fig. 2). The quaternary structure, including the position of each subunit

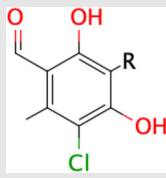
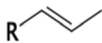
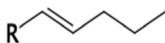
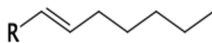
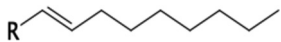
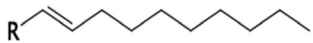

TABLE 2 Inhibition of *E. multilocularis* SQR by derivatives with different substitutions on the benzene group

Compound	Structure	IC ₅₀ (μM)
D5		0.047 ± 0.011
D6		0.210 ± 0.022
D7		0.572 ± 0.81
D8		>10
D9		>10
AF		1.10 ± 0.21
D10		0.55 ± 0.13
D11		>10

(Fp, Ip, CybL, and CybS, which correspond to SDHA, SDHB, SDHC, and SDHD subunits, respectively) and prosthetic groups, was based on the crystal structure of *Ascaris suum* complex II that was reported previously by our group (21–23). The predicted structure showed six membrane spanning α -helices (three helices from each of the CybL and CybS subunits) that act as anchors to the mitochondrial inner membrane and amino acid residues surrounding the quinone binding site (Fig. 2). The binding mode of AF derivative D5, the most potent inhibitor of complex II identified in this study, to the quinone binding site formed by Ip, CybL, and CybS subunits was also investigated. The conformation of the bound D5 was predicted based on a previously reported cocrystal structure of *A. suum* complex II with a flutolanil derivative, NN23 (Nihon Nohyaku Co., Ltd., Japan) (Fig. 3A) (22).

In *E. multilocularis* complex II, the entrance of the quinone binding site was

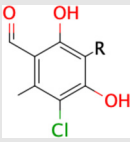
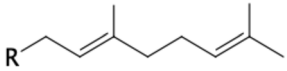
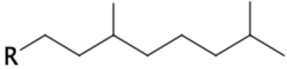
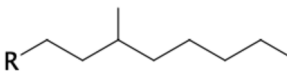
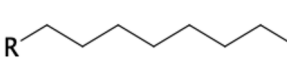
TABLE 3 IC₅₀ against *E. multilocularis* SQR of derivatives with various side chain lengths

R	Compound ID	IC ₅₀ (μM)
	C0	>20
	C3	5.4 ± 0.70
	C5	3.3 ± 0.27
	C7	0.95 ± 0.27
	C9	1.2 ± 0.12
	C10	1.2 ± 0.08
	C12	1.7 ± 0.72

narrowed by the presence of Phe73 at the SDHC subunit (Phe73C), which is replaced by glycine (Gly) in the corresponding subunit from *A. suum* complex II. Also, the calculated entrance sizes of the quinone binding sites of *A. suum* and *E. multilocularis* complex II are 11 × 11 and 6 × 11 Å, respectively. Because of the bulky side chain of the Phe73C residue, our prediction suggests that the quinone binding site of *E. multilocularis* cannot accommodate NN23 (Fig. S2). These observations are further supported by the lack of inhibition of NN23 against *E. multilocularis* complex II (NN23 IC₅₀ > 20 μM), although it strongly inhibited the *A. suum* enzyme at an extremely low concentration, NN23 IC₅₀ = 0.005 μM (Fig. S1). Conversely, D5 strongly inhibited complex II activity of *E. multilocularis* with an IC₅₀ of 0.047 μM, while it showed 234-fold less potent inhibition (IC₅₀ = 11 μM) against *A. suum* complex II activity (Fig. 4). The structure prediction showed that D5 fits tightly into the quinone binding site of *E. multilocularis* complex II, whereas a large empty space is observed between D5 and the pocket inner surface of *A. suum* complex II (Fig. 4), in accordance with the strong and weak inhibition observed for D5 of the respective enzyme activities. Moreover, D5 may interact tightly with the surrounding amino acid residues. The 4-OH of D5 has the potential to form a hydrogen bond with both Tyr107 from the SDHD subunit (Tyr107D) and Trp197 from the SDHB subunit (Trp197B) (Fig. 3A). In addition, the electron-rich guanidino group plane of Arg76 from SDHC (Arg76C) and the electron-deficient benzene plane ring of D5 are placed in parallel, indicating that they might interact strongly with each other via electrostatic interactions (Fig. 3B) (22). Finally, the isoprene chain from bound D5 may be further stabilized through hydrophobic interactions with the benzene ring of Phe73C, which is not conserved in *A. suum* and mammalian complex II, favoring the binding of D5 to *E. multilocularis* complex II (Fig. 3B).

Effects of AF derivatives on the viability of *E. multilocularis* protoscolecocytes in culture assay. A culture assay with protoscolecocytes was performed under aerobic and anaerobic conditions with AF, D2, D4, and D5. As shown in Fig. 5, the viability of the parasites was progressively reduced during *in vitro* treatment with AF under both aerobic and anaerobic

TABLE 4 Inhibition of *E. multilocularis* SQR by different linker structures

Compound ID	Structure	IC ₅₀ (μM)
		
D12		0.57 ± 0.03
D13		0.28 ± 0.05
D14		0.54 ± 0.00
D15		0.89 ± 0.11

conditions. D2 completely eliminated the parasites by day 4 under aerobic culture conditions, while 6 days were required for complete elimination under anaerobic conditions. D4 showed an antiparasitic effect of only 34% elimination on day 7 under aerobic conditions, whereas 65% of the parasites were eliminated by day 7 under anaerobic culture conditions. D5 eliminated the parasites completely by day 6 and day 5 under aerobic and anaerobic conditions, respectively. Thus, D5 killed the parasites more effectively under hypoxia than normoxia.

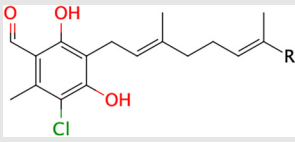
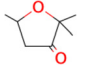
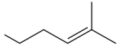
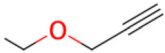
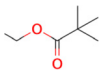
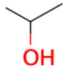
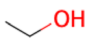
DISCUSSION

In this study, we investigated the effects of AF and its derivatives on the mitochondrial respiratory chain of *E. multilocularis*. Notably, we demonstrated that AF and its derivatives inhibited both complexes II and III of the mitochondrial electron transport chain at submicromolar to nanomolar levels, showing for the first time that simultaneous inhibition of the fumarate and oxygen respiration with a single compound can be achieved. In addition, several AF derivatives are particularly important because they potently inhibited *E. multilocularis* complex II, which is directly involved in the anaerobic respiration maintained by parasites inside the host.

The structure-activity relationship of AF derivatives provided important information about the functional groups crucial for inhibition of *E. multilocularis* complex II, and can be summarized as follows: (i) the 1-acetyl group in the benzene ring improved the inhibition potency compared with a 1-aldehyde group; (ii) the length of the linker required for optimum inhibition was observed to range from C7 to C10, and linkers with two branched methyl groups were preferable; (iii) 5-chlorine is essential for inhibitory activity; and (iv) the 6-methyl group as well as the furanone ring are both dispensable for inhibition; however, depending on the substitution at the terminal group, the inhibitory activity can be increased.

The effect of the AF substituent group structure on enzyme inhibition differs depending on the target. The substitution of the 1-aldehyde group to a 1-acetyl group is deleterious for TAO and HsDHODH inhibitions (15, 24), but seems favorable for inhibition of *E. multilocularis* complex II. A critical role for the 4-OH group in inhibition seems to be a common trait between TAO, HsDHODH, and *E. multilocularis* complex II. Because the removal of the 5-chlorine from the benzene group causes the complete loss of inhibition activity, this group might have an essential interactive role through halogen bonding with εN¹ from Trp197B, similar to what is observed in the cocrystal structures of HsDHODH with AF and its derivatives (15). The 6-methyl group plays an

TABLE 5 *E. multilocularis* SQR inhibition by furanone ring-substituted derivatives

Compound	R	IC ₅₀ (μM)
		
AF		1.10 ± 0.21
D2		0.309 ± 0.021
D16		0.258 ± 0.072
D17		0.488 ± 0.015
D18		3.77 ± 0.98
D19		>10

important role in elevating inhibitory activity for the quinone binding site. This group is required for the optimum inhibition of TAO and HsDHODH (15, 24), but it is dispensable for inhibition of *E. multilocularis* complex II. A plausible explanation is the electron donating nature of the methyl group that induces an electron-rich state of the benzene ring, which reduces the face-to-face parallel interaction with the electron-rich guanidino group of Arg76C, similar to the binding conformation of the trifluoromethylbenzene group of flutolanil derivatives to *A. suum* complex II (22). With respect to the linker group, an unsaturated geranyl linker has been reported to be essential for potent inhibition of TAO (24). However, in *E. multilocularis* complex II, derivatives with saturated linkers, as in D13, were more efficient than D12. Such kinds of derivatives might bind more flexibly to the quinone binding site than derivatives with a geranyl linker. In addition, the furanone ring has previously been found to be dispensable for the strong inhibition of AF and its derivatives against TAO and HsDHODH, although depending on the terminal group, increased inhibition is observed for HsDHODH (15, 24). Similarly, the inhibitory activity for *E. multilocularis* complex II was also increased, but with replacement of different terminal groups compared to the derivatives that increased HsDHODH inhibition (15). Derivatives with saturated linkers, and terminal groups such as O-propynyl (D16), might enable the generation of AF derivatives with greater inhibition efficacy against *E. multilocularis* complex II in the future.

The structure of *E. multilocularis* complex II, modeled based on the crystal structure of *A. suum* complex II (22, 23), suggested a narrow quinone binding site caused by the bulky side chain of Phe73C. This residue appears to be critical for the target specificity of flutolanil and its derivatives, as it causes steric hindrance with the tert-butylbenzene group of NN23, but not with AF derivatives.

Finally, we assessed the effect of AF and its derivatives on *E. multilocularis* protoscolecocytes in a culture assay. We previously hypothesized that a combination of complex II and III inhibitors would inhibit both anaerobic and aerobic respiration, thus killing the

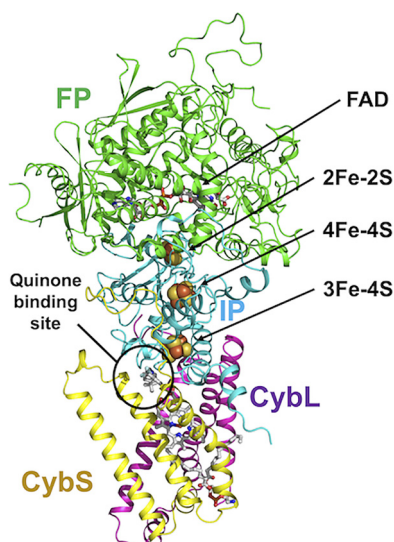


FIG 2 Model structure of *E. multilocularis* complex II using AlphaFold2. Fp (SDHA), Ip (SDHB), CybL (SDHC), and CybS (SDHD) subunits are colored green, cyan, purple, and yellow, respectively. Four prosthetic groups, FAD, [2Fe–2S], [4Fe–4S], and [3Fe–4S], were also modeled based on the reported crystal structures of *A. suum* and porcine complex II.

parasite (6). Culture assay results for AF, D2, and D5 consistently showed a strong anti-parasitic effect on protoscolexes under both anaerobic and aerobic conditions. Although D4 strongly inhibits SQR and succinate-cytochrome c reductase, its effect was weak in the culture assay compared to the other derivatives. It is possible that the structure of the compound may affect cell membrane permeability for drug delivery. Comparing the structure of D2 and D5 with D4, the combination of the 1-aldehyde group in the benzene ring and longer side chain may reduce the cell membrane permeability due to the change in the shape of the structure. However, several novel derivatives might be required to more accurately clarify the cause of the difference between D4 and others, which is a limitation of this study.

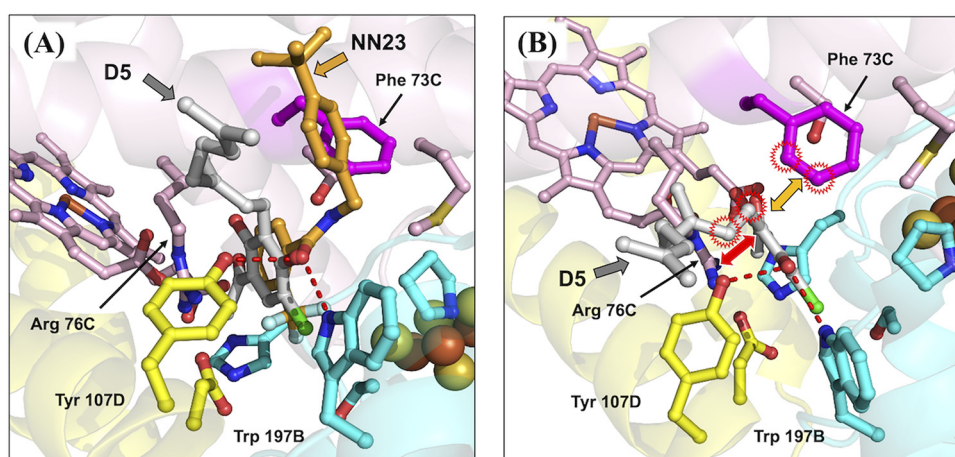


FIG 3 Predicted interaction between AF derivatives and complex II. (A) The position of D5 and a flutolanil derivative (NN23) were merged to predict the interaction between D5 and amino acid residues of *E. multilocularis* complex II based on the cocrystal structure of *A. suum* complex II with NN23. (B) The 4-OH in D5 may contribute to forming hydrogen bonds with both Tyr107D and Trp197B. Hydrogen bonds are represented as red dotted lines. The red double arrow shows the electrostatic interactions between the guanidino group of Arg76C and the benzene ring of D5. The benzene group of Phe73C, which is not conserved in *A. suum* and porcine complex II, might stabilize the binding of D5 by forming hydrophobic interactions with the linker shown as an orange double arrow and red rings.

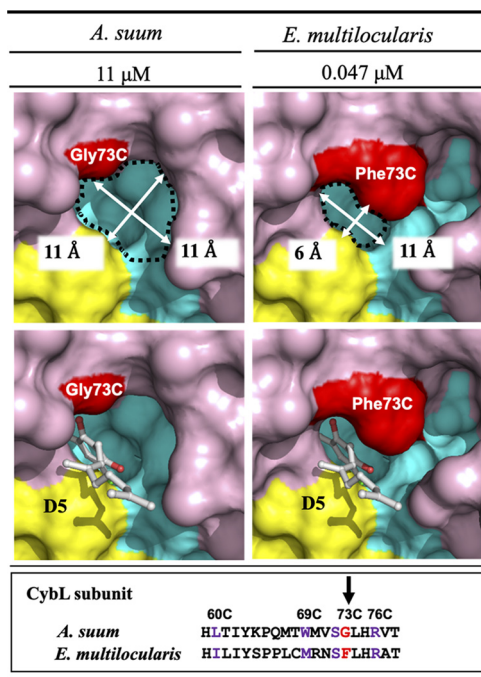


FIG 4 Binding sites of D5 to *A. suum* and *E. multilocularis* complex II and respective IC₅₀ values are denoted. D5 inhibits *E. multilocularis* complex II (IC₅₀ = 0.047 μ M) more strongly than that of *A. suum* (IC₅₀ = 11 μ M). Ip, CybL, and CybS are colored cyan, purple, and yellow, respectively. The Phe73 in CybL and corresponding amino acid residue from *A. suum* are colored red. The dimensions of the entrance to the quinone binding site from *A. suum* and *E. multilocularis* complex II are 11 \times 11 \AA (top left panel) and 6 \times 11 \AA (top right panel), respectively. In the model structure of *E. multilocularis* complex II, D5 fits neatly into the pocket without steric hindrance with Phe73C (bottom right panel), while a large gap between the benzene group of D5 and pocket inner-surface of *A. suum* complex II can be seen (bottom left panel). The bottom of the figure shows a comparison of the amino acid sequences of CybL from *A. suum* and *E. multilocularis*. The arrow indicates that Gly73C from *A. suum* is replaced with Phe73C in *E. multilocularis*.

In the culture assay, the time required to kill protozoa in aerobic and anaerobic conditions differed according to the IC₅₀ value of each compound. For instance, D4 and D5, which inhibited complex II more potently (IC₅₀ = 0.037 and 0.047 μ M) than complex III (IC₅₀ = 0.109 and 0.221 μ M), respectively, showed high killing rates for pro-

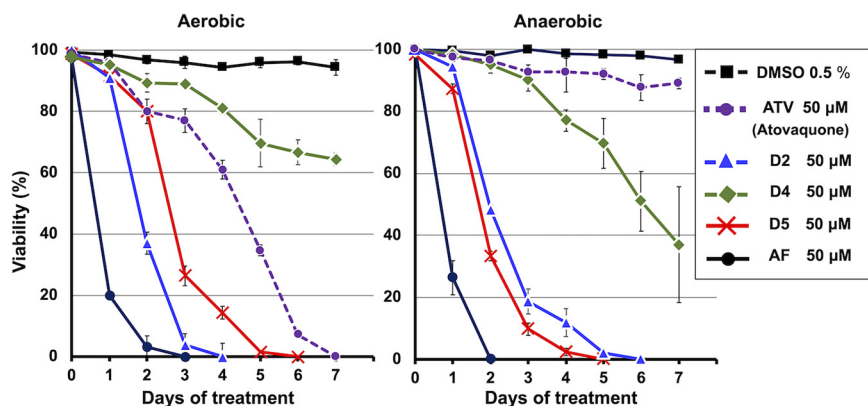


FIG 5 Viability of *E. multilocularis* protozoa in *ex vivo* culture assay. The *E. multilocularis* protozoa were treated with ascofuranone (AF) and its derivatives in culture under aerobic and anaerobic conditions (O₂ < 0.3%). Each compound was added to the culture medium at a final concentration of 50 μ M. The control group was supplemented with 0.5% (vol/vol) dimethyl sulfoxide (DMSO). Atovaquone (ATV) was used as positive control and to ensure anaerobic conditions in the culture. The viability of protozoa was evaluated by their ability to exclude trypan blue. The data are presented as the mean \pm standard deviation ($n = 3$).

toscolecetes under anaerobic conditions compared to aerobic conditions. Also, D2 inhibited *E. multilocularis* complex III with an IC_{50} value of $0.008 \mu\text{M}$, whereas the IC_{50} value for complex II was $0.309 \mu\text{M}$, which indicates that D2 shows a 38-fold higher selectivity for protoscolecetes cultured under aerobic than anaerobic conditions. Interestingly, despite the relatively low inhibitory activity of AF against complex II ($IC_{50} = 1.10 \mu\text{M}$), it exhibited a strong killing effect under anaerobic conditions. This suggests that the furanone ring as the terminal group of AF might contribute to increased cell membrane permeability; however, further studies are required to confirm this hypothesis.

Our findings demonstrate, for the first time, antiparasitic agents that can potentially inhibit both fumarate and oxygen respiration in *E. multilocularis*. The complete blockage of mitochondrial respiration can lead to a pleiotropic effect in the metabolism of all life cycle stages of *E. multilocularis*, including the collapse of the mitochondrial electrochemical gradient, ATP synthesis by oxidative phosphorylation (complex V), the NADH oxidation system (complex I), glycerol metabolism (quinone-dependent mitochondrial glycerol-3-phosphate dehydrogenase), and sulfide metabolism (sulfide:quinone oxidoreductase).

Recently, it was reported that simultaneous inhibition of complex III by ELQ-400 (an endochin-like quinolone) and complex I by quinazoline can enhance the effect of ELQ-400 against the metacestodes of *E. multilocularis* under anaerobic conditions (25). This effect was attributed to the inhibition of aerobic and anaerobic energy metabolism through the inhibition of two respiratory complexes by two different inhibitors. The identification of a single compound simultaneously targeting fumarate and oxygen respiration with potent antiparasitic activity is a unique and groundbreaking feature in the development of novel antiparasitic drugs.

MATERIALS AND METHODS

Preparation of the mitochondrial fraction from *E. multilocularis* protoscolecetes. Cyst tissues containing *E. multilocularis* (Nemuro strain) protoscolecetes isolated from infected hispid cotton rats, *Sigmodon hispidus*, were used. The tissues were shredded through a metal mesh (0.5 mm diameter). Then, the tissues were repeatedly suspended and washed with physiological saline in a tall beaker to obtain protoscolecetes by exploiting the buoyancy difference between protoscolecetes and other tissue (26). The obtained protoscolecetes were homogenized with a motor-driven homogenizer to prepare the mitochondrial fraction. The homogenate was diluted with mitochondrial preparation buffer (210 mM mannitol, 10 mM sucrose, 1 mM disodium EDTA, and 50 mM Tris-HCl [pH 7.5]) supplemented with 10 mM sodium malonate to 5 times the volume of the original protoscolex homogenate, and then centrifuged at $800 \times g$ for 10 min (4°C) to remove cell debris and nuclei. The supernatant was then centrifuged at $8,000 \times g$ for 10 min (4°C) to obtain the mitochondrial pellet. Next, the pellet was resuspended in mitochondrial preparation buffer (without malonate) and centrifuged at $8,000 \times g$ for 10 min (4°C). The enriched mitochondrial fraction was finally suspended in approximately 0.5 to 1.0 mL of mitochondrial preparation buffer without malonate and frozen at -50°C . The mitochondrial fraction from *A. suum* was prepared essentially as described previously (27, 28).

This study was performed in strict accordance with the National Institutes of Health guide for the care and use of laboratory animals. The ethics committee of the Hokkaido Institute of Public Health approved the protocol for the animal experiments (permit numbers: K26-3, K29-4, and K22-1). All surgeries were performed under anesthesia with sodium pentobarbital and isoflurane, and every effort was made to minimize suffering.

Enzyme assays and determination of 50% inhibitory concentration (IC_{50}). NADH:quinone reductase activity (complex I), succinate:quinone reductase activity (complex II), and succinate:cytochrome *c* reductase activity (complexes II to III) were measured using a UV-3000 spectrophotometer (Shimadzu, Kyoto, Japan) as described previously (4, 6). Briefly, all enzyme assays using mitochondrial fractions were performed in 0.5- or 1.0-mL reaction mixtures at 25°C . A freeze/thaw process was performed before the assay to ensure that the mitochondrial membrane was permeable to the solutes. The final mitochondrial protein concentration was $50 \mu\text{g/mL}$. NADH:quinone reductase activity was measured in 50 mM potassium phosphate buffer (pH 7.4) containing 2 mM potassium cyanide, KCN (Sigma, St. Louis, MO, USA), and $60 \mu\text{M}$ decylubiquinone (Sigma). The activity assay was started by the addition of $50 \mu\text{M}$ NADH (Fujifilm-Wako, Tokyo, Japan) and recorded as the rate of NADH consumption as monitored at 340 nm ($\epsilon = 6.2 \text{ mM}^{-1} \text{ cm}^{-1}$). The reagents used in the SQR activity assay were mixed with the reaction buffer containing 50 mM potassium phosphate (pH 7.4) and 0.1% (*wt/vol*) sucrose monolaurate (DOJINDO, Kumamoto, Japan). SQR activity was determined by monitoring the change in absorbance of quinone at 278 nm ($\epsilon = 15 \text{ mM}^{-1} \text{ cm}^{-1}$) in the presence of $60 \mu\text{M}$ decylubiquinone, 2 mM KCN, and the inhibitor. The reaction was initiated by the addition of 10 mM disodium succinate to the mixture. NADH:cytochrome *c* activity (complex I to III) was measured in the reaction buffer (30 mM potassium phosphate, 1 mM MgCl_2 , pH 7.5) containing 2 mM KCN, $50 \mu\text{M}$ cytochrome *c* (Nacal Tesque, Kyoto, Japan), and the inhibitor. The assay was performed after the addition of 100 mM malonate to block complex II

activity. The reaction was started by adding 50 μM NADH to the mixture, and the enzyme activity was determined by monitoring the change in absorbance of cytochrome *c* at 550 nm ($\epsilon = 19 \text{ mM}^{-1} \text{ cm}^{-1}$). IC_{50} values of AF and its derivatives against the specific activities of mitochondrial respiratory enzymes in protoscolecemes were determined. The IC_{50} of each compound was determined by calculating approximation lines from three or more points on either side of the IC_{50} concentration.

Computational crystal structure prediction. We performed protein structure prediction for *E. multilocularis* mitochondrial complex II using AlphaFold2 (29, 30). The docking of four subunits comprising complex II was based on the crystal structure of *A. suum* and porcine complex II described in previous reports (21–23). The prosthetic group of *A. suum* was included in the final model because AlphaFold2 can only predict polypeptide models. The binding mode of an AF derivative (D5) in *E. multilocularis* complex II was predicted based on previous reports of the crystal structure of *A. suum* in complex with flutolanil (22, 31, 32). The protein sequences of *E. multilocularis* complex II subunits were retrieved from the NCBI database using the following accession numbers: Fp (BAX90095.1), Ip (BAX90096.1), CybL (BAX90098.1), and CybS (BAX90099.1).

Culture assays of live *E. multilocularis* protoscolecemes. The obtained protoscolecemes were cultured in Connaught Medical Research Laboratories 1066 medium (Gibco, Grand Island, NY, USA) containing 0.5% (*wt/vol*) yeast extract (Difco Laboratories, Detroit, MI, USA), 2 mM L-glutamine (Gibco), 23 mM 4-(2-hydroxyethyl)-1-piperazineethanesulfonic acid, 0.5% (*wt/vol*) D (+)-glucose, 0.4 mM sodium taurocholate (Wako Pure Chemical Industries, Osaka, Japan), 57 mM sodium hydrogen carbonate, and 100 U/mL penicillin-streptomycin (Gibco). The protoscolecemes were observed daily for seven consecutive days, and half of the medium was replaced on day 3. For anaerobic cultures, six-well plates were sealed in plastic containers with oxygen-detecting agents and oxygen scavengers (Aneromeito, Nissui Pharmaceutical, Tokyo, Japan) to keep the oxygen concentration below 0.3% at 37°C. The protoscolecemes were treated with AF and its derivatives at a final concentration of 50 μM in the culture medium, and the duration of parasite elimination was investigated. The control group was supplemented with 0.5% (*vol/vol*) dimethyl sulfoxide (DMSO), and all conditions were assayed in triplicate. We used ATV in a culture assay as positive control and to ensure anaerobic conditions in the culture (4, 5). The IC_{50} of ATV against SQR and succinate-cytochrome *c* reductase was 0.69 μM and 0.002 μM , respectively. The viability of protoscolecemes was determined after microscopic observation of more than 170 protoscolecemes per well using the trypan blue exclusion test, as described previously (4, 6, 33).

Synthesis of AF and its derivatives. The AF and AF derivatives used in this study were previously designed and synthesized as compounds targeting TAO for anti-trypanosomal drug development (24, 34, 35).

Statistical analysis. The results of IC_{50} and culture assay viability determinations are each expressed as the mean \pm standard error of the mean (SEM). All statistical analyses were performed using EZR (version R3.6.3; Saitama Medical Center, Jichi Medical University, Saitama, Japan) (36).

SUPPLEMENTAL MATERIAL

Supplemental material is available online only.

SUPPLEMENTAL FILE 1, PDF file, 1.5 MB.

ACKNOWLEDGMENTS

We thank Hiroyuki Saimoto and all of the graduate students at the Department of Chemistry and Biotechnology, Graduate School of Engineering, Tottori University for their assistance with the synthesis of AF derivatives.

This work was supported in part by Grants-in-Aid for Scientific Research (B) (No. 16K19114 and 19H03436 to K.K. and D.K.I.), and a grant from The Leading Initiative for Excellent Young Researchers (LEADER; No. 16811362 to D.K.I.) from the Japanese Ministry of Education, Science, Culture, Sports and Technology (MEXT). This work also was supported by a grant from the Japanese Initiative for Progress of Research on Infectious Diseases for Global Epidemics (No. JP18fm0208027 to D.K.I.); and by Grants-in-Aid for research on emerging and re-emerging infectious diseases from the Japanese Ministry of Health, Labor and Welfare (No. JP17fk0108119 to K.K. and No. JP21fk0108138 to D.K.I.); and by KAKENHI of the Japan Society for the Promotion of Science (No. 22K07048 to H.K.).

We declare that we have no known competing financial interests or personal relationships that could have appeared to influence the work reported in this paper.

REFERENCES

1. Wen H, Vuitton L, Tuxun T, Li J, Vuitton DA, Zhang W, McManus DP. 2019. Echinococcosis: advances in the 21st century. *Clin Microbiol Rev* 32: e00075-18. <https://doi.org/10.1128/CMR.00075-18>.
2. Mihmanli M, Idiz UO, Kaya C, Demir U, Bostanci O, Omeroglu S, Bozkurt E. 2016. Current status of diagnosis and treatment of hepatic echinococcosis. *World J Hepatol* 8:1169–1181. <https://doi.org/10.4254/wjh.v8.i28.1169>.
3. Siles-Lucas M, Casulli A, Cirilli R, Carmena D. 2018. Progress in the pharmacological treatment of human cystic and alveolar echinococcosis: compounds and therapeutic targets. *PLoS Negl Trop Dis* 12:e0006422. <https://doi.org/10.1371/journal.pntd.0006422>.
4. Enkai S, Kouguchi H, Inaoka DK, Irie T, Yagi K, Kita K. 2021. In vivo efficacy of combination therapy with albendazole and atovaquone against primary

- hydatid cysts in mice. *Eur J Clin Microbiol Infect Dis* 40:1815–1820. <https://doi.org/10.1007/s10096-021-04230-5>.
5. Enkai S, Inaoka DK, Kouguchi H, Irie T, Yagi K, Kita K. 2020. Mitochondrial complex III in larval stage of *Echinococcus multilocularis* as a potential chemotherapeutic target and in vivo efficacy of atovaquone against primary hydatid cysts. *Parasitol Int* 75:102004. <https://doi.org/10.1016/j.parint.2019.102004>.
 6. Matsumoto J, Sakamoto K, Shinjo N, Kido Y, Yamamoto N, Yagi K, Miyoshi H, Nonaka N, Katakura K, Kita K, Oku Y. 2008. Anaerobic NADH-fumarate reductase system is predominant in the respiratory chain of *Echinococcus multilocularis*, providing a novel target for the chemotherapy of alveolar echinococcosis. *Antimicrob Agents Chemother* 52:164–170. <https://doi.org/10.1128/AAC.00378-07>.
 7. Tsai IJ, Zarowiecki M, Holroyd N, Garciarubio A, Sánchez-Flores A, Brooks KL, Tracey A, Bobes RJ, Fragoso G, Sciuotto E, Aslett M, Beasley H, Bennett HM, Cai X, Camicia F, Clark R, Cucher M, De Silva N, Day TA, Deplazes P, Estrada K, Fernández C, Holland PWH, Hou J, Hu S, Huckvale T, Hung SS, Kamenetzky L, Keane JA, Kiss F, Koziol U, Lambert O, Liu K, Luo X, Luo Y, Macchiaroli N, Nichol S, Paps J, Parkinson J, Pouchkina-Stantcheva N, Riddiford N, Rosenzvit M, Salinas G, Wasmoth JD, Zamanian M, Zheng Y, Cai J, Soberón X, Olson PD, Lactette JP. Taenia solium Genome Consortium, et al. 2013. The genomes of four tapeworm species reveal adaptations to parasitism. *Nature* 496:57–63. <https://doi.org/10.1038/nature12031>.
 8. Hijikawa Y, Matsuzaki M, Suzuki M, Suzuki S, Inaoka DK, Tatsumi R, Kido Y, Kita K. 2017. Re-identification of the ascofuranone-producing fungus *Ascochyta viciae* as *Acremonium sclerotigenum*. *J Antibiot (Tokyo)* 70:304–307. <https://doi.org/10.1038/ja.2016.132>.
 9. Summerbell RC, Gueidan C, Guarro J, Eskalen A, Crous PW, Gupta AK, Gené J, Cano-Lira JF, Iperen AV, Starink M, Scott JA. 2018. The Protean *Acremonium*. *A. sclerotigenum/egyptiacum*: revision, food contaminant, and human disease. *Microorganisms* 6:88. <https://doi.org/10.3390/microorganisms6030088>.
 10. Balogun EO, Inaoka DK, Shiba T, Tsuge C, May B, Sato T, Kido Y, Nara T, Aoki T, Honma T, Tanaka A, Inoue M, Matsuoka S, Michels PAM, Watanabe YI, Moore AL, Harada S, Kita K. 2019. Discovery of trypanocidal coumarins with dual inhibition of both the glycerol kinase and alternative oxidase of *Trypanosoma brucei brucei*. *FASEB J* 33:13002–13013. <https://doi.org/10.1096/fj.201901342R>.
 11. Shiba T, Inaoka DK, Takahashi G, Tsuge C, Kido Y, Young L, Ueda S, Balogun EO, Nara T, Honma T, Tanaka A, Inoue M, Saimoto H, Harada S, Moore AL, Kita K. 2019. Insights into the ubiquinol/dioxygen binding and proton relay pathways of the alternative oxidase. *Biochim Biophys Acta Bioenerg* 1860:375–382. <https://doi.org/10.1016/j.bbabi.2019.03.008>.
 12. Nakamura K, Fujioka S, Fukumoto S, Inoue N, Sakamoto K, Hirata H, Kido Y, Yabu Y, Suzuki T, Watanabe Y, Saimoto H, Akiyama H, Kita K. 2010. Trypanosome alternative oxidase, a potential therapeutic target for sleeping sickness, is conserved among *Trypanosoma brucei* subspecies. *Parasitol Int* 59:560–564. <https://doi.org/10.1016/j.parint.2010.07.006>.
 13. Yabu Y, Suzuki T, Nihei C, Minagawa N, Hosokawa T, Nagai K, Kita K, Ohta N. 2006. Chemotherapeutic efficacy of ascofuranone in *Trypanosoma vivax*-infected mice without glycerol. *Parasitol Int* 55:39–43. <https://doi.org/10.1016/j.parint.2005.09.003>.
 14. Talaam KK, Inaoka DK, Hatta T, Tsubokawa D, Tsuji N, Wada M, Saimoto H, Kita K, Hamano S. 2021. Mitochondria as a potential target for the development of prophylactic and therapeutic drugs against *Schistosoma mansoni* infection. *Antimicrob Agents Chemother* 65:e0041821. <https://doi.org/10.1128/AAC.00418-21>.
 15. Miyazaki Y, Inaoka DK, Shiba T, Saimoto H, Sakura T, Amalia E, Kido Y, Sakai C, Nakamura M, Moore AL, Harada S, Kita K. 2018. Selective cytotoxicity of dihydroorotate dehydrogenase inhibitors to human cancer cells under hypoxia and nutrient-deprived conditions. *Front Pharmacol* 9:997. <https://doi.org/10.3389/fphar.2018.00997>.
 16. Shen W, Ren X, Zhu J, Xu Y, Lin J, Li Y, Zhao F, Zheng H, Li R, Cui X, Zhang X, Lu X, Zheng Z. 2016. Discovery of a new structural class of competitive hDHODH inhibitors with in vitro and in vivo anti-inflammatory, immunosuppressive effects. *Eur J Pharmacol* 15:205–212. <https://doi.org/10.1016/j.ejphar.2016.09.004>.
 17. Jeong YJ, Hwang SK, Magae J, Chang YC. 2020. Ascofuranone suppresses invasion and F-actin cytoskeleton organization in cancer cells by inhibiting the mTOR complex 1 signaling pathway. *Cell Oncol (Dordr)* 43:793–805. <https://doi.org/10.1007/s13402-020-00520-w>.
 18. Kim HW, Jeong YJ, Hwang SK, Park YY, Choi YH, Kim CH, Magae J, Chang YC. 2020. Ascofuranone inhibits epidermal growth factor-induced cell migration by blocking epithelial-mesenchymal transition in lung cancer cells. *Eur J Pharmacol* 5:173199. <https://doi.org/10.1016/j.ejphar.2020.173199>.
 19. Matsuzaki M, Tatsumi R, Kita K. 2017. Protoclerol generation from the ascofuranone-producing fungus *Acremonium sclerotigenum*. *Cytologia* 82:317–320. <https://doi.org/10.1508/cytologia.82.317>.
 20. Araki Y, Awakawa T, Matsuzaki M, Cho R, Matsuda Y, Hoshino S, Shinohara Y, Yamamoto M, Kido Y, Inaoka DK, Nagamune K, Ito K, Abe I, Kita K. 2019. Complete biosynthetic pathways of ascofuranone and ascochlorin in *Acremonium egyptiacum*. *Proc Natl Acad Sci U S A* 116:8269–8274. <https://doi.org/10.1073/pnas.1819254116>.
 21. Sun F, Huo X, Zhai Y, Wang A, Xu J, Su D, Bartlam M, Rao Z. 2005. Crystal structure of mitochondrial respiratory membrane protein complex II. *Cell* 121:1043–1057. <https://doi.org/10.1016/j.cell.2005.05.025>.
 22. Inaoka DK, Shiba T, Sato D, Balogun EO, Sasaki T, Nagahama M, Oda M, Matsuoka S, Ohmori J, Honma T, Inoue M, Kita K, Harada S. 2015. Structural insights into the molecular design of flutolanil derivatives targeted for fumarate respiration of parasite mitochondria. *Int J Mol Sci* 16:15287–15308. <https://doi.org/10.3390/ijms160715287>.
 23. Harada S, Inaoka DK, Ohmori J, Kita K. 2013. Diversity of parasite complex II. *Biochim Biophys Acta* 1827:658–667. <https://doi.org/10.1016/j.bbabi.2013.01.005>.
 24. Saimoto H, Kido Y, Haga Y, Sakamoto K, Kita K. 2013. Pharmacophore identification of ascofuranone, potent inhibitor of cyanide-insensitive alternative oxidase of *Trypanosoma brucei*. *J Biochem* 153:267–273. <https://doi.org/10.1093/jb/mvs135>.
 25. Chaudhry S, Zurbriggen R, Preza M, Kämpfer T, Kaethner M, Memedovski R, Scorrano N, Hemphill A, Doggett JS, Lundström-Stadelmann B. 2022. Dual inhibition of the *Echinococcus multilocularis* energy metabolism. *Front Vet Sci* 9:981664. <https://doi.org/10.3389/fvets.2022.981664>.
 26. Matsumoto J, Kouguchi H, Oku Y, Yagi K. 2010. Primary alveolar echinococcosis: course of larval development and antibody responses in intermediate host rodents with different genetic backgrounds after oral infection with eggs of *Echinococcus multilocularis*. *Parasitol Int* 59:435–444. <https://doi.org/10.1016/j.parint.2010.06.003>.
 27. Takamiya S, Kita K, Wang H, Weinstein PP, Hiraishi A, Oya H, Aoki T. 1993. Developmental changes in the respiratory chain of *Ascaris* mitochondria. *Biochim Biophys Acta* 1141:65–74. [https://doi.org/10.1016/0005-2728\(93\)90190-q](https://doi.org/10.1016/0005-2728(93)90190-q).
 28. Takamiya S, Furushima R, Oya H. 1984. Electron transfer complexes of *Ascaris suum* muscle mitochondria. I. Characterization of NADH-cytochrome c reductase (complex I–III), with special reference to cytochrome localization. *Mol Biochem Parasitol* 13:121–134. [https://doi.org/10.1016/0166-6851\(84\)90107-5](https://doi.org/10.1016/0166-6851(84)90107-5).
 29. Jumper J, Evans R, Pritzel A, Green T, Figurnov M, Ronneberger O, Tunyasuvunakool K, Bates R, Židek A, Potapenko A, Bridgland A, Meyer C, Kohl SAA, Ballard AJ, Cowie A, Romera-Paredes B, Nikolov S, Jain R, Adler J, Back T, Petersen S, Reiman D, Clancy E, Zielinski M, Steinegger M, Pacholska M, Berghammer T, Bodenstein S, Silver D, Vinyals O, Senior AW, Kavukcuoglu K, Kohli P, Hassabis D. 2021. Highly accurate protein structure prediction with AlphaFold. *Nature* 596:583–589. <https://doi.org/10.1038/s41586-021-03819-2>.
 30. Tunyasuvunakool K, Adler J, Wu Z, Green T, Zielinski M, Židek A, Bridgland A, Cowie A, Meyer C, Laydon A, Velankar S, Kleywegt GJ, Bateman A, Evans R, Pritzel A, Figurnov M, Ronneberger O, Bates R, Kohl SAA, Potapenko A, Ballard AJ, Romera-Paredes B, Nikolov S, Jain R, Clancy E, Reiman D, Petersen S, Senior AW, Kavukcuoglu K, Birney E, Kohli P, Jumper J, Hassabis D. 2021. Highly accurate protein structure prediction for the human proteome. *Nature* 596:590–596. <https://doi.org/10.1038/s41586-021-03828-1>.
 31. Delano W. 2004. Use of PyMOL as a communications tool for molecular science. *Abstracts of Papers of the American Chemical Society, Amer Chemical Soc* 228:228–230.
 32. Mooers BHM, Brown ME. 2021. Templates for writing PyMOL scripts. *Protein Sci* 30:262–269. <https://doi.org/10.1002/pro.3997>.
 33. Thompson RC, Deplazes P, Eckert J. 1990. Uniform strobilar development of *Echinococcus multilocularis* in vitro from protoscoleces to immature stages. *J Parasitol* 76:240–247. <https://doi.org/10.2307/3283023>.
 34. Kita K, Inaoka DK, Saimoto H, Yamamoto M. 2012. Dihydroorotic acid dehydrogenase inhibitor. U.S. Patent No. US20150166498A1. Tokyo, Japan.
 35. Saimoto H, Kita K, Yabu Y, Yamamoto M. 2015. Novel dihydroxybenzene derivatives and anti-protozoan agent containing them as active ingredients. Japan Patent No. JP5960300B2. Tokyo, Japan.
 36. Kanda Y. 2013. Investigation of the freely available easy-to-use software 'EZR' for medical statistics. *Bone Marrow Transplant* 48:452–458. <https://doi.org/10.1038/bmt.2012.244>.